International Journal of Mechanical Sciences 93 (2015) 240–255

Contents lists available at ScienceDirect

International Journal of Mechanical Sciences

journal homepage: www.elsevier.com/locate/ijmecsci

Computational homogenisation of periodic cellular materials: Application to structural modelling

A. Iltchev [a], V. Marcadon [a,*], S. Kruch [a], S. Forest [b]

[a] ONERA - The French Aerospace Lab, DMSM, 29 Avenue de la Division Leclerc, BP 72, F-92322 Châtillon Cedex, France
[b] Mines ParisTech, Centre des Matériaux, CNRS UMR 7633, BP 87, F-91003 Evry cedex, France

ARTICLE INFO

Article history:
Received 25 September 2014
Received in revised form
14 January 2015
Accepted 15 February 2015
Available online 21 February 2015

Keywords:
Cellular architectures
Periodic homogenisation
Effective multi-axial behaviour
Elasto-plastic properties
Finite element modelling

ABSTRACT

The present paper aims at investigating the homogenisation of cellular materials in view of the modelling of large but finite cellular structures. Indeed, computation costs associated with the complete modelling of such structures can be rapidly prohibitive if industrial applications are considered. The use of a homogeneous equivalent medium (HEM) for these cellular materials can be an efficient approach to address this issue, but it requires the calibration of relevant homogeneous equivalent laws (HELs). Here, the considered cellular materials are tube stackings. Various uni-axial and multi-axial loading cases have been simulated, through the finite element method, on representative volume elements of such periodic stackings. From these simulations, anisotropic compressible elasto-plastic constitutive equations have been identified for the HEL. The anisotropy of the yield surfaces is discussed depending on the pattern of the tube stacking (e.g. square or hexagonal). A validation of the identified laws is proposed by simulating uni-axial compression and simple shear tests on sandwich structures made of tube stackings for their cores. A systematic comparison, between the results obtained from the fully meshed structures and those obtained from the structures whose core has been replaced with its HEM, allows us to address the limitations of the HEM-based approach and the boundary layer effects observed on finite structures.

1. Introduction

Cellular materials have been widely studied for their various functionalities [1] which make them attractive for numerous applications, for instance in which impact resistance or acoustic absorption is required. From a mechanical point of view, high specific properties relative to the bulk are expected which could be very useful in the development of lightweight aeronautical frames. However, the modelling of such cellular materials presents some difficulties because of the issue of the separation of their different characteristic scales; the size of the constitutive cells is often in the same order of magnitude as the one of the structure. A refined modelling of the mechanical behaviour of these materials is thus necessary to simulate large structures (with many constitutive cells but without increasing the computation costs), but keeping information on the local mechanisms which govern their mechanical behaviour (such as localised plasticity in the cells). To address this issue, a modelling approach based on the identification and the use of a homogeneous equivalent medium is investigated here.

By using a multi-scale description of cellular materials, many authors were interested in the influence of the intrinsic morphological and material parameters of these materials on their effective mechanical properties. For instance, one can cite the works of Silva et al. [2,3], Fazekas et al. [4], Sanders and Gibson [5,6] and Marcadon and Kruch [7] concerning the effect of the architecture or those of Amsterdam et al. [8,9] Mangipudi et al. [10] and Marcadon et al. [11,12] addressing the effect of the constitutive material. Numerous studies investigated also the characterisation of the damage mechanisms which govern the failure of cellular structures, especially the collapse of their constitutive cells [13–16]. The scale transition between both the microscopic and the macroscopic scales allowed authors to study the initial macroscopic plastic yield stress from the first plastic hinge at the microscopic scale, such as proposed by Gasser et al. [17]. Alkhader and Vural [18] studied the beginning of plasticity in foams depending on the topology and the resulting dominant deformation modes. The macroscopic yield and the behaviour of cellular structures in their inelastic domain have been studied too. Experimental campaigns of characterisation have been carried out on various geometries under both quasi-static [19–21] and dynamic [22,23] loads, but also computational characterisations. Full scale models have been developed for various architectures of cellular materials. Depending on the geometry of the cells, authors proposed different models such as beam models at finite strains for Papka and Kyriakides [24], shell models of real geometries coming from tomography analyses for Caty et al. [25], or solid models in 2D or 3D for Marcadon et al. [11,21]. In order to get macroscopic mechanical responses, authors used homogenisation techniques too

* Corresponding author. Tel.: +33 146734524; fax: +33 146734891.
E-mail address: Vincent.Marcadon@onera.fr (V. Marcadon).

http://dx.doi.org/10.1016/j.ijmecsci.2015.02.007
0020-7403/

for non-periodic media, see for instance the work of Ostoja-Starzewski [26].Beam models were used to study the influence of the morphology, i.e. variations of the cell size or geometrical defects and their dispersion, on the elastic properties and the onset of plasticity [27–29]. More complex beam elements were also considered in advanced models in order to better capture the architecture and the local collapse mechanisms [10,30,31].

Cellular materials are increasingly used in large structures. Thus their behaviour under arbitrary load depending on the application has to be known in order to predict the behaviour of whole structures. One can either consider a full-scale model describing all the characteristic scales of the material, but the computation costs become rapidly too expensive. On the contrary, the heterogeneous architecture can be replaced favourably by a homogeneous equivalent medium (HEM) into the modelling [32,33]. However, this technique requires the accurate characterisation of the relation between the macroscopic stresses and strains. It can either be the result of nested finite element simulations and be used in a structural model, or it can be an effective material law. The FE^2 (nested finite element) scheme [34–36] has the advantage to need no assumption on the macroscopic mechanical response, but it remains costly when applied to large 3D structures. On the contrary, the HEM-based modelling is very efficient in terms of computation costs, but it results in a loss of information concerning the architecture of the cellular material and it must be rigorously identified to be relevant. Various macroscopic material models that fit the macroscopic behaviour of cellular materials have been proposed to take into account their compressibility and their anisotropy. They can be identified either from experimental results [37–39] or from periodic simulations as proposed by Tsuda et al. [40]. Depending on their base material properties and their architecture, the homogenised behaviour can be isotropic (mainly for random architectures) or can exhibit an anisotropy if a certain regularity in the organisation or a particular shape of the cells exist. For instance, a quadratic yield criterion has been proposed by Hill [41]. Similarly, several yield criteria were proposed by Karafillis and Boyce [42], Barlat et al. [43] or Bron and Besson [44] to model multi-axial non-quadradic yield flows. Moreover, in the particular case of cellular materials, the void inside or within the constitutive cells leads to the compressibility of the effective behaviour. A combination of both a shear criterion and a trace dependent criterion governing the compressibility was originally proposed by Green [45]. An isotropic compressible criterion was also proposed for metallic foams by Deshpande and Fleck [39], whereas generalisations of Green's quadratic model [45] were introduced by Badiche et al. [46] and Xue and Hutchinson [32] for anisotropic compressible behaviours. As an illustration of HEM-based approaches, Tsuda et al. [40] characterised a plate-fin structure. The multi-axial inelastic behaviour was characterised by simulating mechanical loads controlled in macroscopic strain up to 0.5%. The anisotropy, the compressibility and the strain rate dependence of the structure effective behaviour were studied and then a quadratic homogenised model was identified in both the elastic and the inelastic domains.

The present work aims at investigating the homogenisation of cellular materials too. Compared with the works of the literature aforementioned, higher strain levels are investigated to discuss the quadratic shape or not of the yield surfaces, depending on cellular architecture and stress concentration, and their evolution according to the level of cumulated plastic strain. Focus is also on the use of such HEM in structural modelling and on boundary layer effects. Reference is made to sandwich structures with a cellular core made of stacked tubes as 'model cellular structures'. The tubes are stacked following either a square pattern or a hexagonal one. First, in Section 2 the multi-axial behaviour of the cellular core is characterised through periodic homogenisation and by simulating various multi-axial loading cases on the unit cells of the two different arrangements of tubes considered. The simulations are performed up to 5% of macroscopic strain and a multi-axial representation of the plastic flow surfaces is proposed in the eigen-stress space from large number of finite element simulations. Then, Section 3 is dedicated to the identification of a HEM for each stacking type considered, square or hexagonal. To finish, in Section 4 the HEM identified previously is used for the modelling of finite sandwich structures made of a tube stacking core. A systematic comparison, between the results obtained form the reference calculations on the fully meshed structures (full-scale modelling) and those predicted by replacing the cores of the sandwich structures with their HEM, is proposed with the purpose of evaluating the relevance of the homogenised constitutive equations identified. A parametric study on finite sandwich structures with various core sizes gives an understanding of the influence of the boundary layer effects depending on both the architecture and the size of the core. For this validation step, normal compression and simple shear in the transverse plane of the tubes were considered as loading cases.

2. Periodic homogenisation analysis of cellular structures

In order to study the macroscopic mechanical behaviour of heterogeneous solids with specific architectures such as those of the tube stackings considered here, a characterisation procedure is proposed involving both the finite element (FE) modelling of virtual multi-axial loading tests and periodic homogenisation techniques.

2.1. Homogenisation method

This kind of cellular structure can be analysed by following a standard homogenisation method. Therefore, the macroscopic strain $\underset{\sim}{E}$ and the macroscopic stress $\underset{\sim}{\Sigma}$ are introduced, according to the definition of Hill [47] and Suquet [48] for periodic homogenisation. They derive from the microscopic strain $\underset{\sim}{\varepsilon}$ and the microscopic stress $\underset{\sim}{\sigma}$ obeying Eqs. (1) and (2):

$$\underset{\sim}{\Sigma} = \langle \underset{\sim}{\sigma} \rangle = \frac{1}{V_\Omega} \int_{V_\Omega} \underset{\sim}{\sigma}\, dV_\Omega \tag{1}$$

$$\underset{\sim}{E} = \langle \underset{\sim}{\varepsilon} \rangle = \frac{1}{V_\Omega} \int_{V_\Omega} \underset{\sim}{\varepsilon}\, dV_\Omega \tag{2}$$

with V_Ω denoting the volume of Ω, the domain occupied by the considered unit cell. Note that, if Eqs. (1) and (2) are still valid here because V_Ω contains the porous part of the unit cell, their computation is not so obvious for cellular materials from the finite-element method [49,50]. In fact, whereas the stress in the voids is known (it equals to 0), so that the macroscopic stress can still be computed from Eq. (1), the strain in the voids is unknown. In that case, the macroscopic strain can be computed from the displacements on the corners of the unit cell with suitable multi-point constraints on the remaining parts of the boundaries.

The multi-scale character of the studied cellular structures is used to carry out the averaging procedure; one periodic unit cell is isolated for each stacking pattern as illustrated in solid lines in Fig. 1. Since focus is only on both elastic and plastic mechanical properties here, the periodic unit cells are valid representative volume elements (RVEs) of the considered regular tube stackings [26]. FE simulations were conducted on the RVE of each stacking pattern to characterise their homogenised mechanical behaviour under multi-axial loads. The RVEs were meshed with triangular quadratic elements and the FE code *Z-set* (http://www.zset-software.com/) was used for the simulations. The different modelling assumptions formulated in the present work are listed hereafter.

Owing to the extruded character of the tube stackings only two-dimensional cross sections of the RVEs have been considered

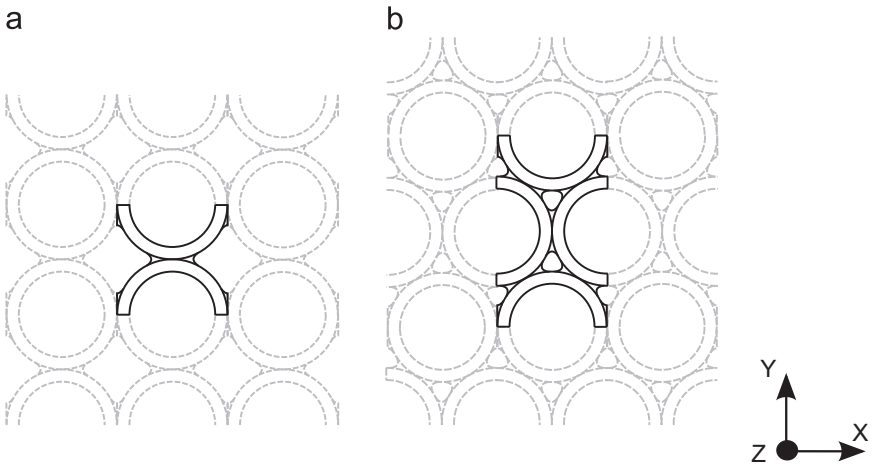

Fig. 1. Unit cells of the periodic tube stackings studied: (a) the square pattern, (b) the hexagonal pattern.

by using generalised plane-strain conditions. Hence it enabled us to simulate both in-plane and out-of-plane mixed loading cases without considering three-dimensional meshes [51]. To apply the periodic boundary conditions, linear multi-point constraints were imposed on the periodic components of the total displacement field on the pairs of opposite nodes on the boundary of the RVEs. The periodic components of the displacements were also set to zero on the unit cell vertices to fix rigid body motions. A small deformation formulation was adopted too for the range of macroscopic strain studied (up to 5%). The periodic homogenisation formulation implemented in *Z-set* allows us to prescribe either macroscopic strains or macroscopic stresses [34].

To illustrate the homogenisation approach described in the present paper, the constitutive material has been assumed to be homogeneous in the tubes and in the braze joints on the basis of our previous works on brazed tube stackings made of nickel-based superalloys [12,21]. Its mechanical properties were identified by performing tensile tests on single tubes after the brazing heat treatment (see [12,21] for more details concerning the processing of such tube stackings and the mechanical characterisation of their constitutive material). The constitutive material is assumed to exhibit an isotropic linear elasticity (Hooke's law) and an isotropic non-linear plasticity governed by the von Mises yield criterion. The classic additive decomposition of the total strain $\underset{\sim}{\varepsilon}$ into an elastic part $\underset{\sim}{\varepsilon}^e$ and a plastic one $\underset{\sim}{\varepsilon}^p$, i.e. $\underset{\sim}{\varepsilon} = \underset{\sim}{\varepsilon}^e + \underset{\sim}{\varepsilon}^p$, is assumed. The constitutive equations of the bulk metal model are the following:

$$\underset{\sim}{\varepsilon}_e = \frac{1+\nu}{E}\underset{\sim}{\sigma} - \frac{\nu}{E}\,\mathrm{tr}(\underset{\sim}{\sigma})\,\underset{\sim}{I} \tag{3}$$

and

$$\dot{\underset{\sim}{\varepsilon}}_p = \dot{\lambda}\frac{\partial \mathcal{F}}{\partial \underset{\sim}{\sigma}} \tag{4}$$

where $\dot{\lambda}$ is the scalar plastic multiplier and $\underset{\sim}{I}$ is the second-order identity tensor. E and ν denote Young's modulus and Poisson's ratio of the constitutive material, respectively. The yield function is

$$\mathcal{F}(\underset{\sim}{\sigma}, p_m) = \sqrt{\frac{3}{2}\underset{\sim}{\sigma}_D : \underset{\sim}{\sigma}_D} - r(p_m) \tag{5}$$

with $\underset{\sim}{\sigma}_D$ being the deviatoric part of $\underset{\sim}{\sigma}$, $\underset{\sim}{\sigma}_D = \underset{\sim}{\sigma} - (1/3)\,\mathrm{tr}(\underset{\sim}{\sigma})\,\underset{\sim}{I}$, and p_m the cumulated plastic strain,

$$p_m = \int_0^t \sqrt{(2/3)\,\dot{\underset{\sim}{\varepsilon}}_p : \dot{\underset{\sim}{\varepsilon}}_p}\, dt \tag{6}$$

The instantaneous yield stress $r(p_m)$ varies according to the following relation:

$$r(p_m) = \sigma_y + h p_m + q(1 - \exp(-b p_m)) \tag{7}$$

with σ_y and h denoting the initial yield stress and the hardening modulus of the constitutive material, respectively. q and b are the material parameters of the non-linear hardening term. The different material parameters used are listed in Table 1.

Table 1
Mechanical properties used for the constitutive material (coming from [12]).

Young's modulus, E (MPa)	171,900
Poisson's ratio, ν	0.3
Initial yield stress, σ_y (MPa)	160.8
Hardening modulus, h (MPa)	1974
Non-linear hardening parameters, q (MPa), b	46.5, 76.2

In the present paper a fixed geometry has been considered for both stackings. The external diameter of the tubes and their thickness are equal to 5 mm and 500 μm, respectively, whereas the length of the braze joints is 1 mm. For this set of geometrical parameters, the ratio of matter is about 29% for the square stacking and 32% for the hexagonal one.

2.2. Homogenised uni-axial mechanical responses

The first step for the numerical mechanical characterisation consisted in the FE simulation of uni-axial tests on the RVEs of the tube stackings. Uni-axial tensions in both the *X*- and *Y*-directions (axes are defined in Fig. 1) have been performed as well as *XY*-plane shear up to 5% of total strain (as illustrated in Fig. 2 for the square stacking and in Fig. 3 for the hexagonal stacking). Uni-axial tensile tests along the out-of-plane *Z*-direction have been performed too for the same level of strain.

From the different uni-axial tensile and simple shear tests simulated, the elastic moduli have been identified first from purely elastic simulations, in order to avoid a plastic contribution that can occur even for very low strain levels due to stress concentration observed for cellular structures. The effective elastic behaviour of the stackings is defined by Hooke's law for linear anisotropic elasticity:

$$\underset{\sim}{\Sigma} = \underset{\approx}{C} : \underset{\sim}{E}_e \tag{8}$$

where $\underset{\approx}{C}$ and $\underset{\sim}{E}^e$ denotes the effective stiffness tensor and the elastic part of the macroscopic strain tensor, respectively. The different components identified for $\underset{\approx}{C}$ are given in Table 2 for both stacking patterns.

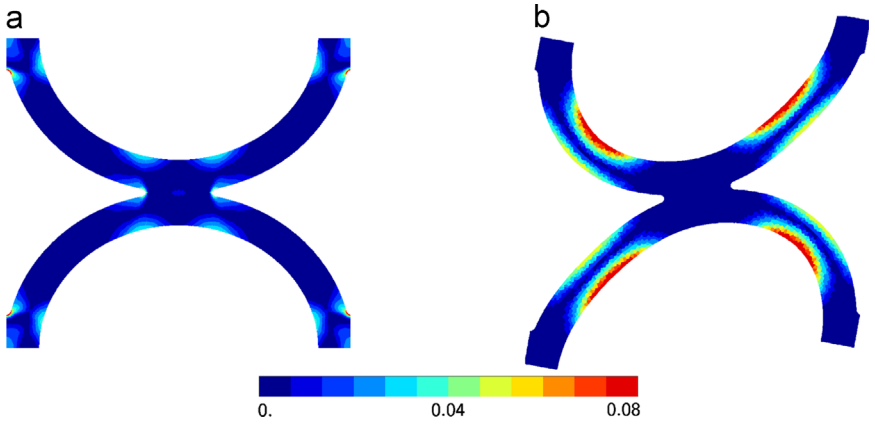

Fig. 2. Von Mises stress maps obtained for the square stacking for a macroscopic strain of 5%: (a) uni-axial tension along the *X*-direction (a similar map is obtained for the tension along the *Y*-direction but rotated with an angle of 90°), (b) simple shear in the *XY*-plane. The maps are plotted in terms of integration node values.

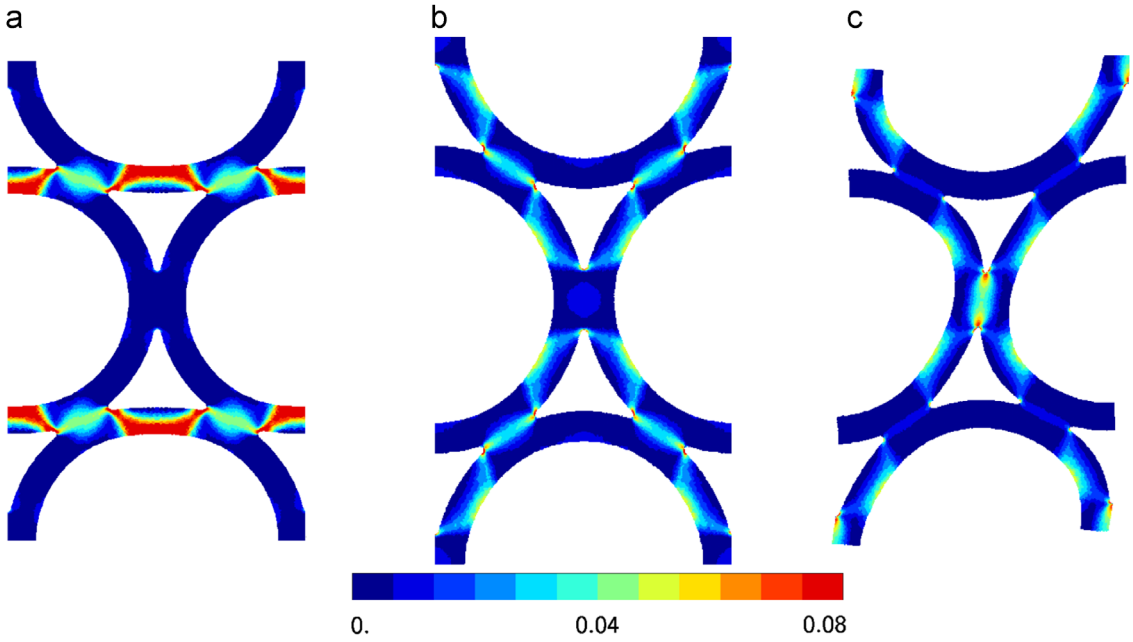

Fig. 3. Von Mises stress maps obtained for the hexagonal stacking for a macroscopic strain of 5%: (a) uni-axial tension along the *X*-direction, (b) uni-axial tension along the *Y*-direction, (c) simple shear in the *XY*-plane. The maps are plotted in terms of integration node values.

The results of the homogenisation procedure exhibit a non-linear and a strongly anisotropic behaviour in the case of the elasto-plastic simulations (see Fig. 4), whatever the loading case is. The main anisotropy comes from the extruded character of the tube stackings; the whole cross-section is homogeneously deformed in the *Z*-direction and the tube stacking behaves similar to its constitutive material to within a factor that equals approximately the fraction of matter present in the cross-section. The in-plane directions, *X*- and *Y*-directions show non-linear behaviours for both types of stacking. It is the result not only of the non-linear behaviour of the base material, but also of the microscopic stress concentration in the tube walls and around the braze joints. The *X*- and *Y*-directions are equivalent in the case of the square stacking, leading to the same mechanical responses in both directions as illustrated in Fig. 4(a). On the contrary, the hexagonal stacking shows an additional in-plane plastic anisotropy (see Fig. 4(b)). The orientation of the braze joints relative to the load direction in this particular stacking is different for each in-plane direction, hence different concentrations of the microscopic stress induce an earlier plastic yield in the neighbourhood of the braze joints for a tensile test along the *X*-direction than along the *Y*-direction. The macroscopic mechanical response of the hexagonal stacking along the *Y*-direction for uni-axial tension is therefore stronger than that along the *X*-direction. However, the hexagonal stacking remains isotropic in terms of in-plane elasticity.

Table 2
Elasticity moduli identified by periodic homogenisation (MPa). The lower indexes 1, 2 and 3 refer to the *X*-, *Y*- and *Z*-directions of Fig. 1, respectively. The components C_{2323} and C_{3131} are not available because of the generalised plane-strain formulation used for the simulations.

$\underset{\approx}{C}$ component (MPa)	Square stacking	Hexagonal stacking
$C_{1111} = C_{2222}$	7555	25,462
C_{3333}	51,688	63,329
$C_{1122} = C_{2211}$	6744	9476
$C_{2233} = C_{3311}$	4292	10,490
C_{1212}	2200	8010

The square and hexagonal stackings show a rather similar strength along the out-of-plane direction (the fractions of matter in the cross-sections of the RVEs equal to about 29 and 32% for the square and the hexagonal stackings, respectively). On the contrary, the strength of the square stacking along the in-plane directions is considerably lower than that of the hexagonal stacking. The

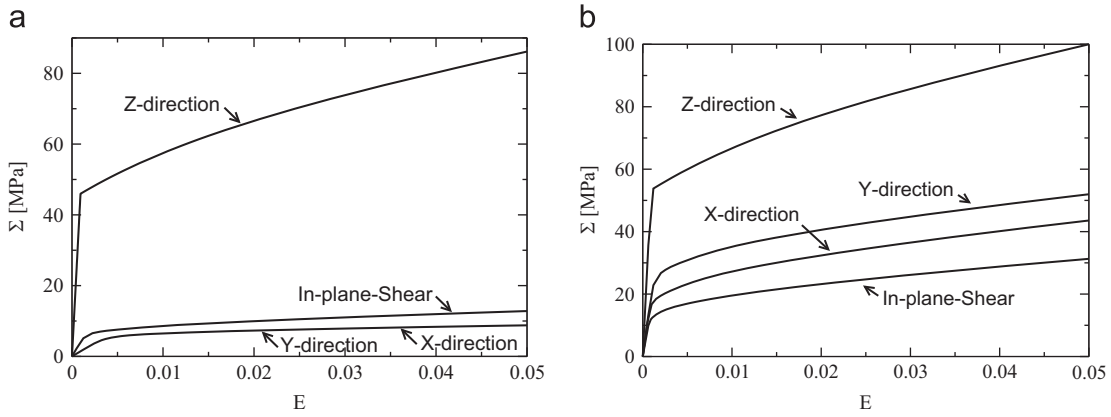

Fig. 4. Mechanical responses for the uni-axial tensile tests along the *X*-, *Y*- and *Z*-directions, and the simple shear in the *XY*-plane, (a) for the square stacking, (b) for the hexagonal stacking.

in-plane/out-of-plane anisotropy is considerably higher for the square stacking. Braze joints have a stiffening effect on tube walls; they are more numerous for the hexagonal stacking, thus they are closer from ones to each others on a tube wall. Hence, the specific density is not necessary the most relevant geometrical parameter to explain the evolution of the mechanical properties of cellular structures [7,11]. It can be also noticed that, the in-plane shear strength of the square stacking is higher than its in-plane tensile strength, which is not the case for the hexagonal stacking.

2.3. Planar bi-axial yield surfaces

The anisotropy of the plastic responses and their evolutions as a function of the loading path have then been characterised for each stacking pattern by a large number of FE simulations of bi-axial tensions. The yield surfaces have been built by simulating proportional loading paths in the space of the principal macroscopic stresses. Indeed, in a chosen $\Sigma_a\Sigma_b-$plane, where Σ_a and Σ_b are the principal components of the bi-axial loading, proportional loading paths can be set for a discrete number of θ ranging in $[0, 2\pi]$:

$$\begin{cases} \Sigma_a = \Sigma_0 \cos\theta \\ \Sigma_b = \Sigma_0 \sin\theta \end{cases} \tag{9}$$

with Σ_0 denoting the amplitude of the bi-axial load. According to the additive decomposition of the total macroscopic strain $\underset{\sim}{E}$ into an elastic part and a plastic one, the macroscopic plastic strain $\underset{\sim}{E}_p$ can be computed from relation:

$$\underset{\sim}{E}_p = \underset{\sim}{E} - \underset{\approx}{C}^{-1} : \underset{\sim}{\Sigma} \tag{10}$$

As already mentioned, the macroscopic plasticity results from both the constitutive material (through its plastic properties) and the architecture of the cellular structure (due to stress concentration) [10,21]. Thus a measure of the macroscopic cumulated plastic strain p has been chosen to parametrise the evolution of the hardening behaviour:

$$p = \int_0^t \sqrt{\frac{2}{3}\dot{\underset{\sim}{E}}_p : \dot{\underset{\sim}{E}}_p}\, dt \tag{11}$$

The macroscopic stress controlled proportional loading paths provide the minimal macroscopic cumulated plastic strain for a given macroscopic stress state. It is the shortest path to reach a point on the actual yield surface.

Various threshold values of $p = p_1, p_2 \ldots p_n$ have been set and for each one the corresponding macroscopic stress state was returned (see Fig. 5). An iterative routine was applied for a finer convergence toward the imposed thresholds. Both in-plane and combinations of in-plane and out-of-plane bi-axial loading cases have been simulated first on the RVEs. Iso-value surfaces of the macroscopic cumulated plastic strain have thus been drawn by assembling the results of the simulated multi-axial tests obtained by varying the value of θ in the range of $[0, 2\pi]$. The surfaces obtained in this way for each p_n have then been considered as macroscopic yield surfaces. The steps of θ depend on the local curvature of the yield surface; it varies from 0.5° where the curvature is high to 10° for a low curvature. The yield surfaces obtained for both stacking patterns are illustrated in Figs. 6 and 7 for threshold values for $p = 0.002$, 0.02 and 0.05.

The analysis of the yield surfaces is in accordance with the results coming from the uni-axial characterisation, see Figs. 4(a) and 6(a) for the square stacking or Figs. 4(b) and 7(a) for the hexagonal one. They provide the same information for these particular loading cases. Figs. 6 and 7 highlight the anisotropy of the in-plane and out-of-plane behaviours for both stackings. Especially, the strong out-of-plane anisotropy observed results from the extruded character of the tube stackings and their higher strength along the *Z*-direction. Similar anisotropic behaviours have been already observed by Sanders and Gibson [5,6] on regular hollow-sphere stackings. However, some differences exist between the square stacking behaviour and that of the hexagonal stacking. Indeed, because of the equivalent roles of the *X*- and *Y*-directions for the square stacking, the yield surfaces exhibit a symmetric shape close to be elliptic but elongated along the axis for which $\Sigma_1 = \Sigma_2$. This is never the case for the hexagonal stacking in which the yield surfaces have non-quadratic shapes. However, the quadratic description or not of the yield surfaces remains a rather complex issue. As described below (see Section 3), even though the shape of the yield surfaces remains non-quadratic in all cases for the hexagonal stacking, if the yield surfaces are plotted in 2D in terms of plastic work density rather than cumulated plastic strain, those of the square stacking exhibit a quadratic shape. Thus, we suppose that the non-quadratic shape of the yield surfaces is intrinsic to the hexagonal stacking. It can be explained by the architecture; the localisation of the plasticity in the neighbourhood of the braze joints first and then in the tube walls govern the direction of the plastic flow and its evolution. On the contrary, the pointed shape of the yield surfaces observed for the square stacking in 3D may result from out-of-plane plastic Poisson's ratio effects. For both stackings, a non-homothetic evolution of the yield surfaces according to the cumulated plastic strain is observed. Such an evolution is a sign of the compressibility of the materials enhanced by their anisotropy. It implies that in the yield criterion chosen the equivalent stress must be a non-linear function of not only the deviatoric part of the stress tensor, but also of its hydrostatic part to account for this compressibility.

2.4. General multi-axial loading cases

This section aims at generalising the method used previously for the characterisation of the planar bi-axial yield surfaces to 3D multi-axial ones. Only the initial yield surface $p=0.002$ has been represented for that purpose. This new representation of the yield surface provides additional information regarding the compressibility of the tube stackings under tri-axial loading, and its anisotropy. The loading paths simulated were no longer proportional but, instead, a pre-load up to a macroscopic hydrostatic stress state then followed by a multi-axial loading path along the radii of the deviatoric planes have been applied to the RVEs. The deviatoric planes are those having the hydrostatic Σ_h-axis as normal, i.e. the planes in which $\Sigma_1=\Sigma_2=\Sigma_3$. Assuming that the macroscopic behaviour is purely elastic up to the yield stress allows the use of non-proportional loading paths. To characterise the evolution of the three-dimensional yield surfaces, we could have considered a projection of the loading paths onto a system of spherical coordinates, similar to the method used before to obtain the planar bi-axial yield surfaces. But it would have required too many simulations.

Fig. 8 shows that the obtained 3D yield surfaces are closed along the spherical part of the macroscopic stress. The tips of the yield surfaces showing the compressible plastic behaviour are not centred around the hydrostatic Σ_h-axis because of the higher strength along the Z-direction characterising both the square and the hexagonal stackings. It can be also noticed that the surfaces are rather flat in the $\Sigma_h\Sigma_3-$plane, especially for the square stacking. Moreover, the near-vertical edge of the yield surfaces under macroscopic hydrostatic loading illustrates the very high yield stress along the out-of-plane direction.

3. Identification of homogeneous equivalent laws

After having characterised the anisotropic elasto-plastic behaviour of both the square and the hexagonal stackings, focus is now on the construction of homogeneous equivalent laws (HELs) of these cellular architectures. They have to gather the distinctive features observed previously from the simulations on the RVE, such as their anisotropic elasticity and anisotropic compressible plasticity. We first start with the identification of a yield criterion for the square stacking and then address the case of the hexagonal stacking. Both stackings have some features in common but they differ regarding the equivalent stress measure involved in the yield function.

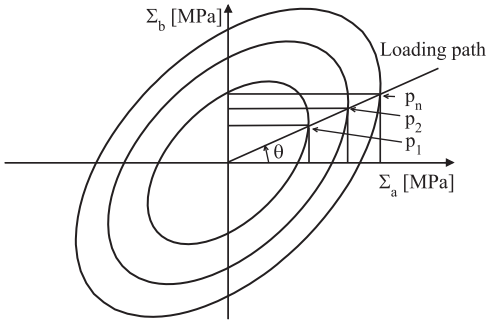

Fig. 5. Construction method of the yield surfaces.

3.1. Square stacking

3.1.1. Formulation of the yield criterion

The total macroscopic strain $\underset{\sim}{E}$ is additively decomposed in the same manner as before (Eq. (10)), i.e. with an elastic part $\underset{\sim}{E}^e$ obeying Eq. (8) and a plastic part $\underset{\sim}{E}_p$ obeying an associated plastic flow rule:

$$\dot{\underset{\sim}{E}}_p=\dot{\lambda}\frac{\partial \mathcal{G}}{\partial \underset{\sim}{\Sigma}} \tag{12}$$

with $\dot{\lambda}$ being the scalar plastic multiplier and $\mathcal{G}$ being the plastic potential written as $\mathcal{G}(\underset{\sim}{\Sigma},p)=\Sigma_{eq}-R(p)$. An elliptic anisotropic criterion, based on Green's one [45] and proposed by Badiche et al. [46], is chosen as yield criterion:

$$\Sigma_{eq}^2=3C\Sigma_e^2+F\Sigma_m^2 \tag{13}$$

where C and F are scalar material coefficients and where Σ_m denotes the modified trace of $\underset{\sim}{\Sigma}$.

$$\Sigma_m=c_1\Sigma_{11}+c_2\Sigma_{22}+c_3\Sigma_{33} \tag{14}$$

with c_1, c_2 and c_3 three scalar material coefficients expressing the anisotropy of the compressibility. It is worth noting that a general form of such an anisotropic compressible yield criterion has been proposed by von Mises [52] by considering an equivalent stress depending on the stress tensor as a whole, including the hydrostatic part, and not on its deviatoric part on one side and on its trace on the other side.

The criterion is written in a general way from the literature and the F parameter of Eq. (13) sets the sensitivity to a hydrostatic stress state. In the anisotropic formulation, F becomes redundant with the coefficients on the components of the trace of the macroscopic stress tensor, hence F is set to 1. Eq. (13) is also function of an equivalent shear stress Σ_e. Since in the case of the square stacking a close to quadratic plastic behaviour has been observed, an equivalent stress of Hill [41] has been chosen:

$$\Sigma_e=\sqrt{\frac{3}{2}\left(\underset{\sim}{\Sigma}_D:\underset{\approx}{H}:\underset{\sim}{\Sigma}_D\right)} \tag{15}$$

where $\underset{\sim}{\Sigma}_D$ denotes the macroscopic deviatoric stress tensor, $\underset{\sim}{\Sigma}_D=\underset{\sim}{\Sigma}-(1/3)\,\mathrm{tr}(\underset{\sim}{\Sigma})\,\underset{\sim}{I}$, and $\underset{\approx}{H}$ is Hill's fourth-order diagonal tensor governing the anisotropy. An equivalent macroscopic cumulated plastic strain p has been defined from Eq. (12) as $\dot{p}=\dot{\lambda}$ assuming an associated plastic flow and the equality of the

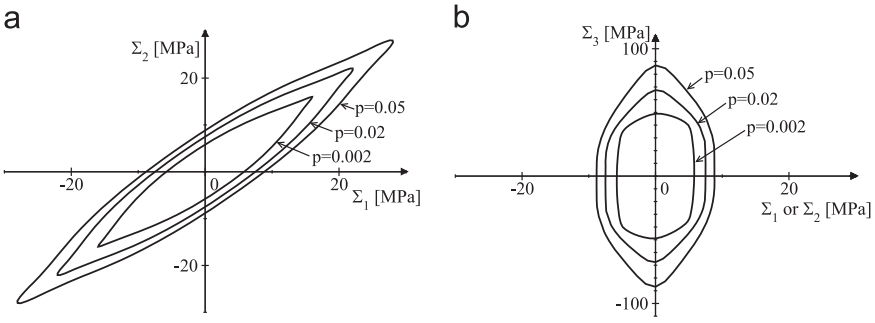

Fig. 6. Planar yield surfaces for the square stacking: (a) $\Sigma_1\Sigma_2-$plane, (b) $\Sigma_1\Sigma_3-$plane (or $\Sigma_2\Sigma_3$).

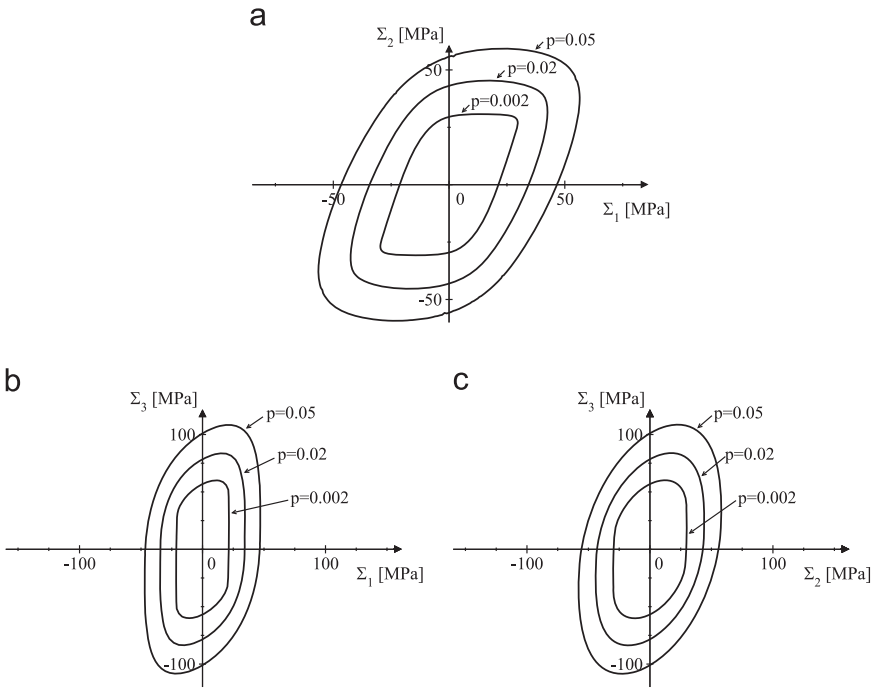

Fig. 7. Planar yield surfaces for the hexagonal stacking: (a) $\Sigma_1\Sigma_2-$plane, (b) $\Sigma_1\Sigma_3-$plane, (c) $\Sigma_2\Sigma_3-$plane.

macroscopic plastic dissipation [46]:

$$\underset{\sim}{\Sigma} : \underset{\sim}{\dot{E}}_p = \Sigma_{eq}\dot{p} \tag{16}$$

The effective hardening $R(p)$ of the cellular structure is non-linear isotropic with the form:

$$R(p) = \Sigma_y + Hp + Q_1(1-\exp(-B_1 p)) + Q_2(1-\exp(-B_2 p)) \tag{17}$$

where Σ_y and H denotes the initial effective yield stress and the effective hardening modulus. The Q_i and B_i are the parameters of the effective non-linear hardening terms. An additional non-linear exponential term has been added compared to the constitutive material in order to account for the non-linearities induced by the architecture.

3.1.2. *Effective mechanical properties*

After having defined the formalism of the homogeneous equivalent law, the different effective parameters have been identified from the simulated uni-axial tensile tests, the shear test and the in-plane bi-axial yield surface. The elastic moduli have been identified first from the extension and shear tests, as mentioned previously. They are given in Table 2. However, the identification of the effective plastic properties is more complex and, because of the number of parameters, a numerical fitting procedure has been carried out.

The shear coefficient of Hill's tensor H is multiplied by the scalar C. Since C is in relation with Σ_e in Eq. (13), it gives the ratio of sensitivity to the spherical and deviatoric parts of the macroscopic stress respectively onto the plastic behaviour. Hence H_{1212} has also been assumed to equal to 1. The c_3 parameter, controlling the out-of-plane compressibility for a hydrostatic stress state has been set to 0 due to the negligible yielding observed along the Z-direction under a spherical load (see Fig. 8). In-plane pure shear, uni-axial and in-plane equi-bi-axial tensions have then been used to determine the unknown material parameters that remained. The in-plane shear stress–strain curve has been used in order to determine the C parameter. The $\underset{\approx}{H}$ components governing the anisotropy, the c_1 and c_2 parameters of the anisotropic compressibility and the hardening parameters have been determined by fitting the stress–strain responses of the uni-axial and equi-bi-axial tensions. In addition, the in-plane transverse macroscopic strain of the uni-axial tension has been used to fit the local plastic flow direction. A numerical optimisation has been carried out with the *Z-opt* module of *Z-set* by using a Levenberg–Marquardt algorithm. The constitutive model parameters identified are given in Table 3.

The identified HEL has been validated by applying it on a single integration point in the *Z-sim* behaviour simulation module of *Z-set* and by simulating the different uni-axial and bi-axial loading cases considered previously for the characterisation of the behaviour of the square stacking RVE. Since they have been used as reference loading cases in the fitting procedure, the uni-axial tensions and in-plane shear show a very good agreement between the mechanical responses of the RVE and those of its HEM (see Fig. 9). The anisotropy as well as the non-linearity of the in-plane behaviour of the RVE of the square stacking are well described by its HEL. The out-of-plane non-linear behaviour predicted by the HEL shows the right trend too, but the fit is not as good as the in-plane ones due to the different origins of the effective non-linear behaviour. Indeed, the non-linearity resulting from the architecture can be neglected in the case of the out-of-plane behaviour of the stacking which is governed by that of its constitutive material only. Thus, the supplementary non-linear isotropic hardening term (Q_2, B_2) added to correctly capture the in-plane behaviour is detrimental to fit the out-of-plane behaviour. The bi-axial yield surfaces in the $\Sigma_1\Sigma_2-$plane are presented in terms of iso-surfaces of density of plastic work, $W_p = \int_0^t \underset{\sim}{\Sigma} : \underset{\sim}{\dot{E}}_p \, dt$, in Fig. 9 too. This measure has been chosen in order to present the results independently from the form of the HEL yield criterion. The yield surfaces show a very good agreement between the mechanical responses of both the RVE and the HEM. The uni-axial extension stress–strain responses are equal in both the X- and Y-directions and the quadratic form of the yield surfaces under a bi-axial stress state is well captured. The hardening is also well modelled owing to the two non-linear exponential hardening terms. In the case of coupled in-plane/out-of-plane stress states the HEL identified fits quite well the behaviour too, in terms of stress state and plastic flow direction.

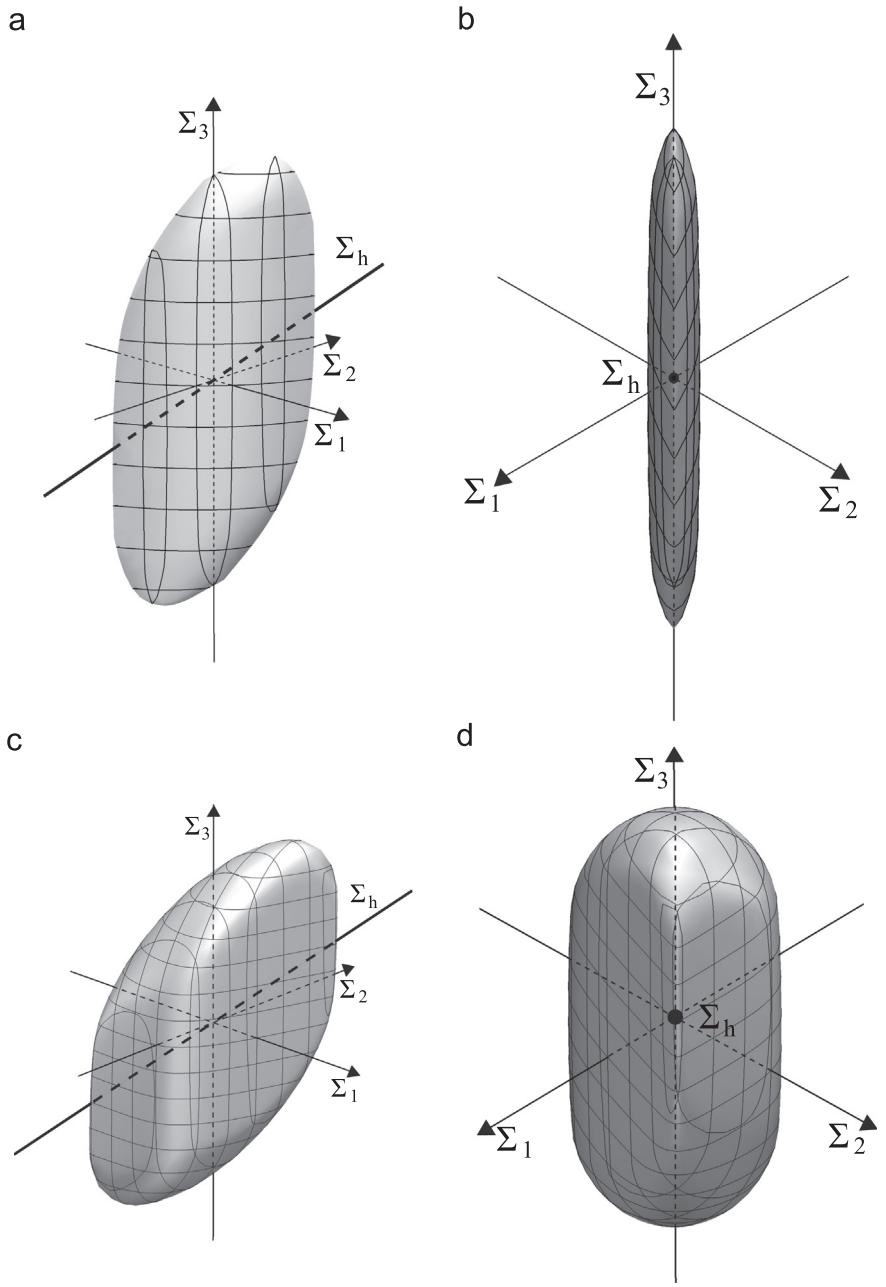

Fig. 8. Initial $p=0.002$ three-dimensional yield surfaces in the space of the macroscopic stresses: (a) and (b) for the square stacking, (c) and (d) for the hexagonal stacking. For the sake of clarity, there are no units on the axes and the reader has to refer to Figs. 6 and 7 for the values for the square and the hexagonal stackings, respectively. However, the shapes of the three-dimensional yield surfaces illustrated in this figure are not distorted ones; the scale is the same for all the axes.

Table 3
Effective plastic properties identified for the square stacking. Similar to the C_{2323} and C_{3131} components of the stiffness tensor, the H_{2323} and H_{3131} components of Hill's tensor are not available because of the generalised plane-strain formulation used for the simulations.

Green's criterion		Hill's tensor		Isotropic hardening	
C	1.8	H_{1111}	5.2	Σ_y (MPa)	10
F	1	H_{2222}	5.2	H (MPa)	161
c_1	0.58	H_{3333}	−2.5	Q_1 (MPa), B_1	5.5, 97
c_2	0.58	H_{1212}	1	Q_2 (MPa), B_2	6.5, 2700
c_3	0				

However, Fig. 10(a) shows that according to the uni-axial tensile simulations the evolution of the hardening along the Z-direction is not as well fitted as in the in-plane directions.

To discuss the choice of the representation of the yield surfaces in terms of plastic work density here rather than in terms of cumulated plastic strain, a comparison between the mechanical responses of the HEM identified for the square stacking and those coming from the simulations on the RVE is illustrated in Fig. 10 (b) in terms of cumulated plastic strain in the plane $\Sigma_1\Sigma_2$. In fact, the classical cumulated plastic strain has been chosen a priori as a representative measure of the plastic behaviour of the tube stackings in the first part of this work because of their unknown behaviour. However, regarding the complex form of the yield criterion identified and especially the strong in-plane/out-of-plane anisotropy, the use of the cumulated plastic strain presents some problems since it accounts for an out-of-plane plastic strain even for a pure in-plane loading. The sharp shape of the yield surfaces observed for an in-plane bi-axial loading results from the out-of-plane plastic Poisson's effect and is very difficult to capture. For

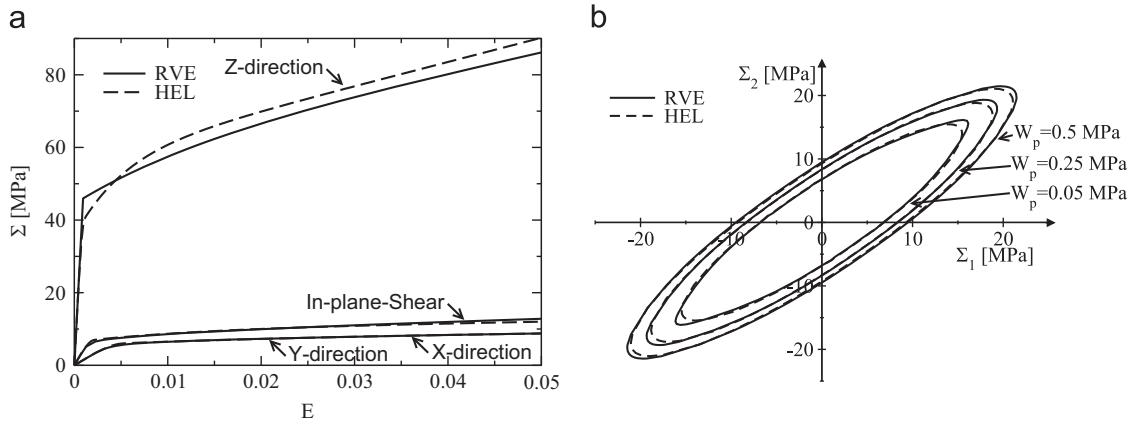

Fig. 9. Comparison between the mechanical responses of the HEM identified for the square stacking and those coming from the simulations on the RVE: (a) in terms of uni-axial tensions and in-plane shear, (b) in terms of the $\Sigma_1\Sigma_2-$in$-$plane surfaces of plastic work density.

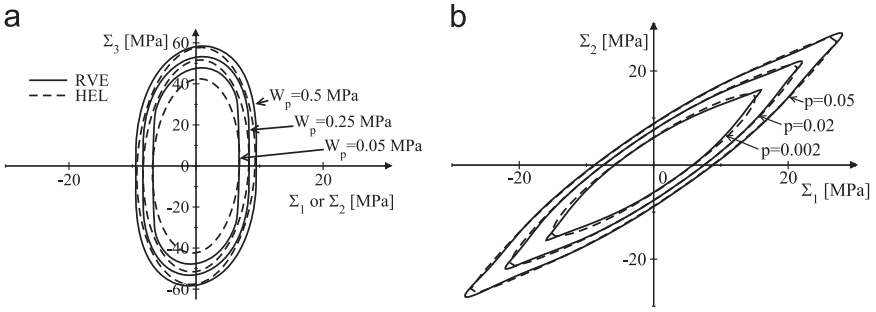

Fig. 10. Comparison between the mechanical responses of the HEM identified for the square stacking and those coming from the simulations on the RVE: (a) in terms of the $\Sigma_1\Sigma_3-$out$-$of $-$ plane surfaces of plastic work density, (b) in terms of the $\Sigma_1\Sigma_2-$in$-$plane surfaces of cumulated plastic strain.

this reason, the density of plastic work is a very convenient measure to overcome this difficulty.

3.2. Hexagonal stacking

As shown into the work of Tsuda et al. [40], Hill's criterion does not suit to capture non-quadratic yield surfaces. A good agreement can be obtained when fitting the uni-axial mechanical responses only but not when considering multi-axial loading cases in the general case of cellular materials with a non-quadratic behaviour [27,38,40]. Thus, the hexagonal stacking must be modelled with a more complex yield criterion.

3.2.1. Formulation of the yield criterion

The macroscopic model chosen for the hexagonal stacking still follows Eqs. (13), (14) and (17) regarding compressibility and hardening. However, the equivalent shear stress is now governed by a general non-quadratic yield function according to Bron and Besson [44]:

$$\Sigma_e = [\alpha((\psi^1)^{1/b^1})^a + (1-\alpha)((\psi^2)^{1/b^2})^a]^{1/a} \tag{18}$$

with a, α, b^1, b^2 being scalar material coefficients. Functions ψ^1 and ψ^2 obey

$$\begin{cases} \psi^1 = \dfrac{1}{2}(|S_2^1 - S_3^1|^{b^1} + |S_3^1 - S_1^1|^{b^1} + |S_1^1 - S_2^1|)^{b^1}) \\ \psi^2 = \dfrac{3^{b^2}}{2^{b^2}+2}(|S_1^2|^{b^2} + |S_2^2|^{b^2} + |S_3^2|^{b^2}) \end{cases} \tag{19}$$

where the $S_{i=1-3}^{k=1-2}$ denote the principal values of two different stress deviators $\underset{\sim}{\Sigma}_D^{k=1-2}$ defined as

$$\underset{\sim}{\Sigma}_D^k = \underset{\approx}{B}^k : \underset{\sim}{\Sigma} \tag{20}$$

and where

$$\underset{\approx}{B}^k = \begin{pmatrix} (c_2^k + c_3^k)/3 & -c_3^k/3 & -c_2^k/3 & 0 & 0 & 0 \\ -c_3^k/3 & (c_3^k + c_1^k)/3 & -c_1^k/3 & 0 & 0 & 0 \\ -c_2^k/3 & -c_1^k/3 & (c_1^k + c_2^k)/3 & 0 & 0 & 0 \\ 0 & 0 & 0 & c_4^k & 0 & 0 \\ 0 & 0 & 0 & 0 & c_5^k & 0 \\ 0 & 0 & 0 & 0 & 0 & c_6^k \end{pmatrix} \tag{21}$$

An equivalent macroscopic cumulated plastic strain p is defined from Eq. (12) as $\dot{p} = \dot{\lambda}$ assuming an associated plastic flow and Eq. (16) [44]:

$$\underset{\sim}{\Sigma} : \underset{\sim}{\dot{E}}_p = \Sigma_{eq}\dot{p} \tag{22}$$

Many other phenomenological yield functions exist in the literature [42,43], but the one proposed by Bron and Besson has been preferred because of its general character that enables us to capture a large variety of behaviours, anisotropic and quadratic or not.

3.3. Effective mechanical properties

The procedure used to identify the constitutive parameters of a HEL for the hexagonal stacking is similar to the one described previously in Section 3.1.2 for the square stacking. The components of the effective stiffness tensor have been identified first as already mentioned (see Table 2 in Section 2.2). The c_3 parameter in Eq. (14) has been set to 0 (for the same reasons as in the case of the square stacking). Concerning the shear behaviour, the c_6^1 and c_6^2 components of the $\underset{\approx}{B}^1$ and $\underset{\approx}{B}^2$ tensors have been set to 1. In-plane pure shear, uni-axial and in-plane equi-bi-axial tensions have then been used to determine the remaining unknown material parameters.

The in-plane shear stress–strain curve has been used for the identification of the C parameter. The anisotropy parameters of the $\underset{\approx}{B}^1$ and $\underset{\approx}{B}^2$ tensors associated with tensions and those governing the compressibility, c_1 and c_2, have been calibrated by fitting both the uni-axial and the equi-bi-axial tensions with the mechanical responses of the HEM. The transverse strains have also been used in order to capture the local plastic flow direction. The set of parameters identified is given in Table 4. It is worth noting that, because of the numerous parameters of the model, this set of values is not unique. The results of the fitting procedure obtained for the hexagonal stacking are illustrated in Fig. 11.

The comparison between the mechanical responses of the HEM and those obtained from the FE simulations on the hexagonal RVE shows reasonably close results (see Fig. 11). The bi-axial yield surfaces in the XY-plane are presented in Fig. 11 too, with the same graphic representation as the one used for the square stacking (see Section 3.1.2). The anisotropy as well as the non-linearity of the in-plane behaviour of the hexagonal stacking are successfully captured by the fitted HEL. However, when the load state is a mixed one, with both in-plane and out-of-plane components, the model displays some limitations due to the plastic transverse strain (not illustrated here). The results could be improved by using a multi-potential yield criterion that could be more accurate but more complex too [53]. In addition, although the non-linear hardening is fairly well modelled as a whole, in the particular case of the hexagonal stacking some difficulties are encountered when trying to capture perfectly the mechanical responses of bi-axial loading cases. An additional anisotropy might be introduced on the hardening, and not only on the yield criterion, but it would require even more parameters. Thus we have preferred to keep the aforementioned model that contains many parameters yet and the Y-direction has been favoured in the fitting procedure for the hexagonal stacking. This is according to the cases of validation of the identified HEL considered for the simulation of sandwich structures and described next in Section 4. Fig. 11 illustrates the fact that both the hardening evolution and the normal to the flow surface are correctly captured around the Y-axis.

Even if the corresponding fitted properties are not given in Table 4 for the sake of brevity, we have tried to fit the homogenised behaviour of the hexagonal stacking by using Hill's equivalent stress rather than Bron–Besson's one, such as for the square stacking. However, the fitted yield surfaces have been added in Fig. 11(b). As mentioned before and according to the results of Tsuda et al. [40], Hill's criterion permits us to capture uni-axial tensions but is not sufficient to correctly capture the complex shape of the yield surface and the right direction of the plastic flow locally in the case of a multi-axial loading.

Comparisons between the mechanical responses of the HEM identified for the hexagonal stacking and those coming from the simulations on the RVE are illustrated in Fig. 12 in terms of the $\Sigma_1\Sigma_3-\text{out}-\text{of}-\text{plane}$ and $\Sigma_2\Sigma_3-\text{out}-\text{of}-\text{plane}$ surfaces of plastic work density. Similar to those obtained for the square stacking, these comparisons assert the difficulty of capturing well the in-plane behaviour and the out-of-plane one simultaneously, despite the complex yield function considered here. In fact, neither Hill's equivalent stress nor the one of Bron and Besson succeed in reaching a close fit of the simulated yield surfaces.

Table 4
Effective plastic properties identified for the hexagonal stacking. Similar to the C_{2323} and C_{3131} components of the stiffness tensor, the c_4^1, c_5^1, c_4^2 and c_5^2 components of $\underset{\approx}{B}^1$ and $\underset{\approx}{B}^2$ tensors are left undetermined because of the generalised plane-strain formulation used for the simulations.

Green's criterion		Bron-Besson's tensors				Isotropic hardening	
C	2	b^1	3	b^2	2	Σ_y (MPa)	33
F	1	c_1^1	0.81	c_1^2	0.02	H (MPa)	410
c_1	0.69	c_2^1	0.15	c_2^2	0.85	Q_1 (MPa), B_1	19, 71
c_2	0.63	c_3^1	0.93	c_3^2	1.31	Q_2 (MPa), B_2	4.8, 1050
c_3	0	c_6^1	1	c_6^2	1		
		a	17.4				
		α	0.524				

4. Modelling of sandwich structures

The purpose now is the evaluation of the HELs identified before for both stacking types for the modelling of finite sandwich structures. The sandwich structures considered are made of upper and lower skins with a tube stacking core in between. Reference full-scale computations on fully meshed sandwich structures have been performed first. The inhomogeneity of both the stress and strain fields in the architectures, under uni-axial normal compressive and in-plane simple shear loads, has been analysed. It has permitted us to discuss the replacement of the stacking core with its HEM into the modelling. Boundary layer effects resulting from the finite size of the sandwich core on the mechanical responses of the sandwich structures are addressed for both stacking types. Similar to the simulations on RVEs of the tubes stackings (see Section 2), simulations on the sandwich structures have been performed by using quadratic triangles and the finite-element software *Z-set*.

4.1. Geometries and models

Various sandwich structures have been considered for the validation step of the HELs. These different structures are summarised in Fig. 13. For all the simulated sandwich structures, the geometrical parameters (e.g. the tube thickness and external diameter, and the braze length) are kept constant and are the same as those used for the identification of the HELs. The thickness of the skins of the sandwich structures is fixed to 1 mm. The only parameter that changes from one architecture to another is the size of the core. It is defined by its numbers of whole tubes in the width and in the height. The constitutive material properties are also the same as those used previously for the characterisation of the infinite tube stackings. Both square of hexagonal tube stackings are considered.

In the case of the square stacking, the definition of the sandwich structures has been straightforward since the modelled structure is representative of a real one that would have been processed by stacking and brazing the tubes between two skins in one step [21]. For this structure, except for the free lateral edges, all the core can be considered as periodic. Each tube has the same number of neighbour tubes, hence the same number of braze joints equal to 4. Moreover, this number is the same as the one in the RVE of the stacking.

The case of the hexagonal stacking is a little bit more complex and two different architectures must be considered. The first architecture simulated is illustrated in Fig. 14(a). Similar to the square stacking, we have considered an architecture in which each tube in the sandwich contains the same number of neighbour tubes as the one in the RVE, hence the same number of braze joints that equals 6 for this stacking. It corresponds to a pseudo-periodic core with cut peripheral tubes. However, this architecture is not representative of a real structure that would have been processed in one step by stacking the tubes between the skins. Thus the second architecture made of full peripheral tubes, and illustrated in Fig. 14(b), has been studied too in order to discuss boundary layer effects. The peripheral tubes are not represented by the periodic unit cell of the stacking because they do not have

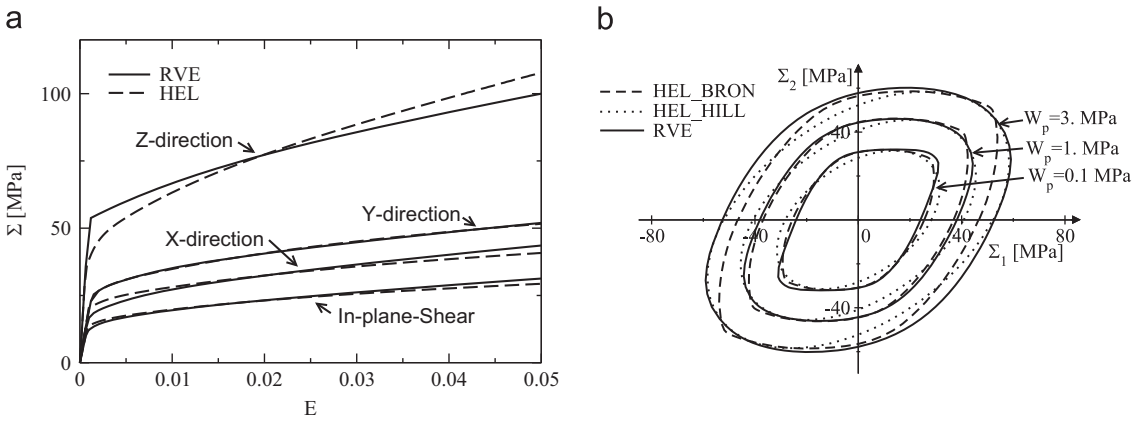

Fig. 11. Comparison between the mechanical responses of the HEM identified for the hexagonal stacking and those coming from the simulations on the RVE: (a) in terms of uni-axial tensions and in-plane shear, (b) in terms of the $\Sigma_1\Sigma_2-$in$-$plane surfaces of plastic work density.

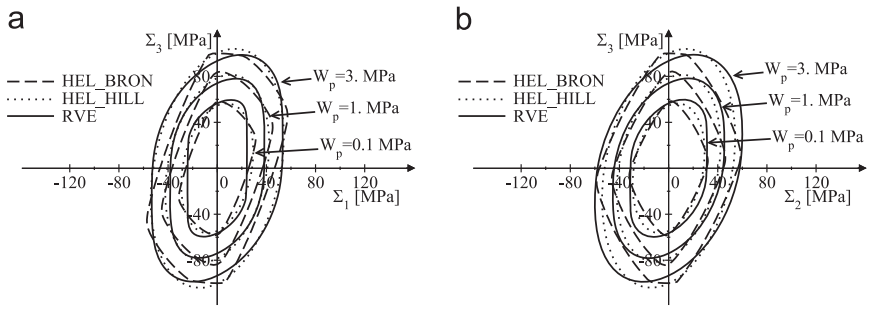

Fig. 12. Comparison between the mechanical responses of the HEM identified for the hexagonal stacking and those coming from the simulations on the RVE: (a) in terms of the $\Sigma_1\Sigma_3-$out$-$of $-$ plane surfaces of plastic work density, (b) in terms of the $\Sigma_2\Sigma_3-$out$-$of $-$ plane surfaces of plastic work density.

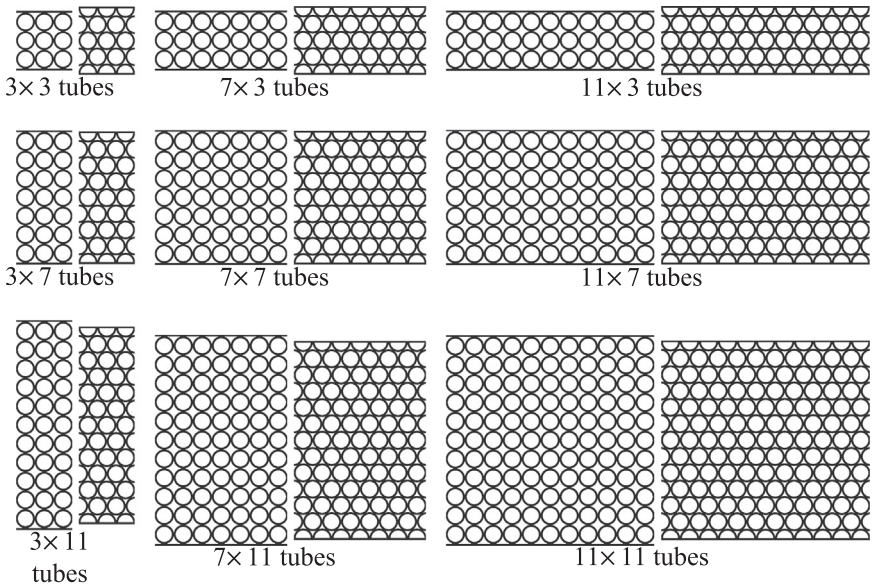

Fig. 13. Illustrations of the various sandwich structures simulated in the case of a fully periodic core (square stacking on the left, hexagonal one on the right).

all their neighbouring tubes, hence a lower strength is expected from this region of the core.

In parallel to this full-scale modelling, models of the sandwich structures aforementioned have been proposed by replacing their cores by their HEM. The aim was to considerably decrease computational costs in view of structural modelling. The scale transition between the cellular cores and their HEM has been made by using the macroscopic laws identified from the homogenisation approach. This modelling strategy can be applied when the load is not local [54]. It means that the multi-axial stress state must evolve in space more slowly than the characteristic length of the cellular architecture (or the explicit heterogeneity in a more general point of view in heterogeneous materials) in order to respect the scale separation assumption. Both the square stacking structure and the first hexagonal one (architecture shown in Fig. 14(a)) could be described as finite periodic cores except for the lateral faces of the sandwich structures. Thus we have assumed in both cases that the tube stacking cores could be replaced in the whole by their HEM. The lateral free surfaces of the cores have been modelled as free

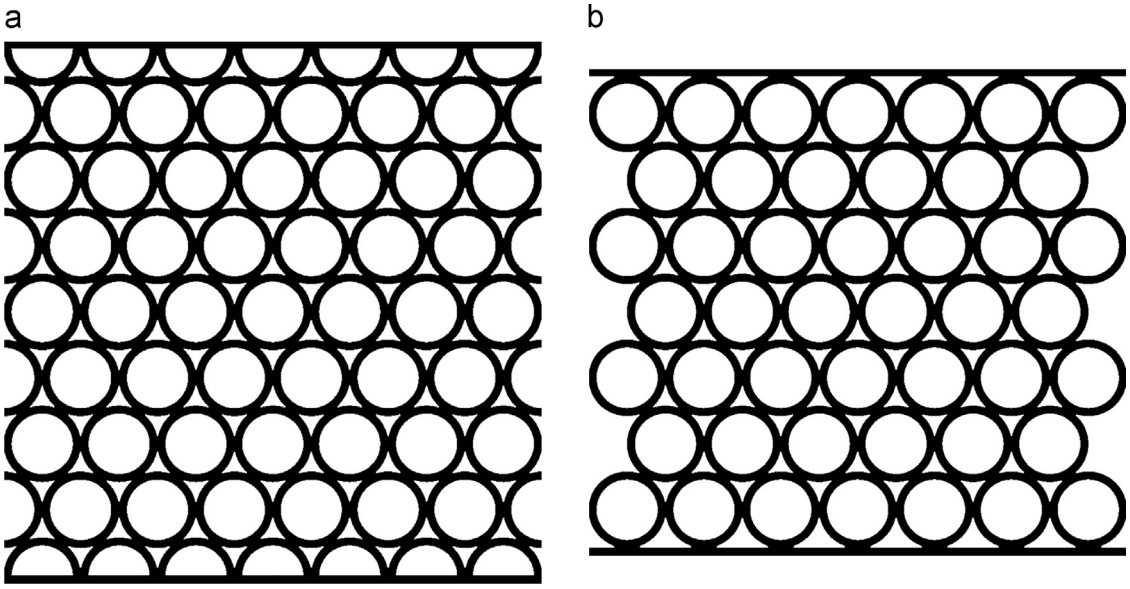

Fig. 14. The two different sandwich structures studied with a hexagonal core: (a) periodic core. (b) technological geometry, i.e. compact stacking of tubes between the face skins.

surfaces in the HEM-based simulations, such as in the full-scale ones.

On the contrary, when considering the technological structures for the hexagonal stacking illustrated in Fig. 14(b), the results obtained from the full-scale simulations have shown that the core can no longer be replaced by its HEM as a whole. It is due to the preferential collapse of the tubes in contact with the skins. Therefore, in that case the peripheral half-tubes have been kept fully meshed and only the central periodic region of the core has been replaced by the HEM. The interface between these two domains, i.e. the fully meshed half-tubes and the HEM of the core, is not continuous and the large strength difference between the constitutive material of the tubes and the HEM results in an indentation of the HEM by the tube walls. In order to avoid the occurrence of this modelling artefact, a uniform displacement condition normal to the interface between the half-tubes meshed and the HEM has been applied on several nodes of the outer edges of the HEM around the tube walls. This complementary modelling assumption is in rather good agreement with the displacement fields observed on the reference full-scale simulations. However, some steps are observed on the deformed geometries between the regions where the uniform displacement condition is applied and those where node displacements remain free. A localisation of the strain is observed at these steps but this modelling artefact remains very localised and does not affect significantly the macroscopic mechanical response of the sandwich structures. A compromise has been found in terms of the width of interface areas enabling us to minimise the displacement gradient but without having a too strong indentation of the HEM. The width equals to one third of the internal diameter of the tubes on both sides of them; it corresponds to about four elements each time. Thus, between two tube wall junctions with the HEM, the central third of the edges of the HEM is deformed freely. In the case of the in-plane shear load of the cellular structures, the displacement is approximated by steps as illustrated in Fig. 15. More complex interface conditions exit in the literature, such as the ones proposed by Panasenko [55] and based on the decomposition of the border of the domain in several sub-domains in which higher order homogenised conditions are applied. However, for the sake of simplicity, a uniform displacement condition has been preferred here since it provides accurate enough results.

4.2. Results and boundary layer effects

Uniform compressive and simple shear loads have been applied on the sandwich structures by imposing displacements to their skins. Multi-axial stress states in the core of the sandwich structures are observed due to the heterogeneous interfaces between the core and both the lower and the upper skins. Moreover, in spite of the absence of internal length-scale in the HEM-based modelling developed in the present work, the macroscopic mechanical responses of the structures vary with respect to the size of their core because of the difference in mechanical strength between the skins and the core. The different mechanical responses predicted by both the full-scale modelling and those HEM-based are compared in Figs. 17–21. They are presented in terms of nominal stress vs. nominal strain curves in order to consider quantities that are not dependent on the size of the core of the sandwich structure.

The reference full-scale simulations have been analysed first. In the case of the square stacking they show in Fig. 16 a decreasing effective strength of the sandwich structure with respect to an increasing core size when there are as many tubes in the height as in the width. However, this general trend has to be reconsidered if the aspect ratio of the core (i.e. the ratio between the number of tubes in the height and in the width) is not equal to 1, as illustrated in Fig. 17. For a fixed height of the core, the macroscopic strength of the sandwich structure increases with the width of the core (Fig. 17(a)). This edge effect is the result of the containment role of the skins. In contrast, for a constant sandwich width, an increase of the number of tubes in the height of the core results in a decrease of the macroscopic strength of the sandwich due to the lateral free edges of the structure as illustrated in Fig. 17(b). The decrease in macroscopic strength observed for sandwich structures with an aspect ratio of 1 when increasing the core size (Fig. 16) suggests that the boundary layer effect that mainly governs the sandwich structure behaviour is associated with the lateral free edges. For this particular stacking, a pronounced barrel shape is observed systematically under compression as illustrated in Fig. 18(a). If the HEM-based simulations are now considered for the square stacking (see Fig. 18(b)), they show rather satisfactory results for modelling the behaviour of the sandwich structures except for the smaller core size. Fig. 16 shows a convergence in

terms of macroscopic mechanical response between the full-scale simulations and those HEM-based with respect to the core size of the sandwich structure. Such a conclusion is true not only in the case of a compressive load, but also in the case of a simple shear one.

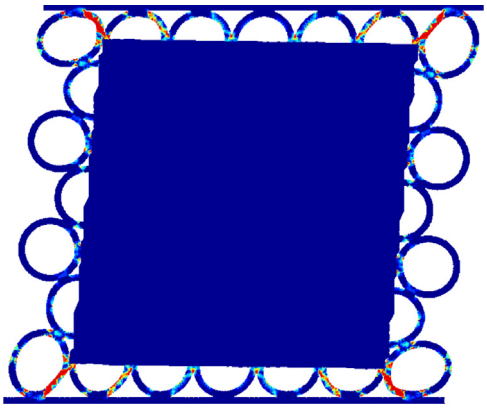

Fig. 15. Illustration of the problem of the junction between the peripheral meshed half-tubes and the homogenised core in the case of the technological hexagonal specimen. This cumulated plastic strain map has been obtained in the case of an in-plane shear load for the 7×7-hexagonal stacking core. The map is plotted in terms of integration node values.

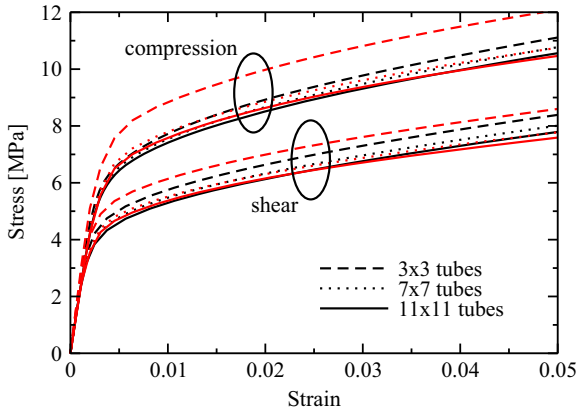

Fig. 16. Comparison between the mechanical responses predicted by both the full-scale modelling (black curves) and the HEM-based one (red curves) in the case of the square stacking core, for both compressive and simple shear loads. (For interpretation of the references to colour in this figure caption, the reader is referred to the web version of this paper.)

The case of the sandwich structures made of a hexagonal stacking core is more complex. If the sandwich structure with a pseudo-periodic hexagonal core is considered first, the various full-scale simulations performed on this structure by varying its core size lead to the same conclusions as those aforementioned for the square stacking core (see Fig. 20). Furthermore, even if the gap between the mechanical responses predicted from the full scale models and those HEM-based is larger than that observed for the square stacking (HEM-based modelling tends to systematically overestimate the mechanical response for the hexagonal stacking), the core size effect is well predicted. However, Fig. 21(a) shows an increasing strength for the sandwich structure when increasing the core size, for an aspect ratio close to one. Therefore, in contrast to the square stacking, the boundary layer effect that mainly influences the mechanical response of the sandwich structure is the confinement effect of the skins. Indeed, the barrel shape of the deformed structure under compression remains small compared to that one observed for the square stacking core (Fig. 19). The mechanical responses predicted by the HEM-based simulations converge to those obtained from the reference full-scale simulations (Fig. 21(a)).

The hexagonal stacking with whole peripheral tubes shows very different trends due to the additional non-periodicity of the core. The observation of the deformed maps reveals a strong localisation of the collapse of the tubes that mainly occurs in the peripheral tubes. This reduces significantly the strength of the core but the effect saturates when increasing the core size (see Fig. 21 (b)). In that particular case, replacing the whole core with its HEM leads to overestimate the mechanical response by the HEM-based modelling, as illustrated in Fig. 21 in the case of a compressive load. In contrast, a rather good agreement is obtained between the results predicted by both the full-scale modelling and the HEM-based one if only the periodic domain of the core is replaced with its HEM and the half-tubes at the periphery are kept meshed. This modelling strategy is a little bit less efficient to reduce computation costs and despite the very good agreement with the full-scale model for the compressive load, it shows some limitations for the simple shear load. It might be due to the use of a too simple displacement boundary condition at the interface between the peripheral tubes and the HEM to avoid its indentation. This issue must be investigated deeper to improve our approach [55].

5. Conclusion

The present work aimed at investigating the relevance of homogenisation approaches for the modelling of finite size cellular

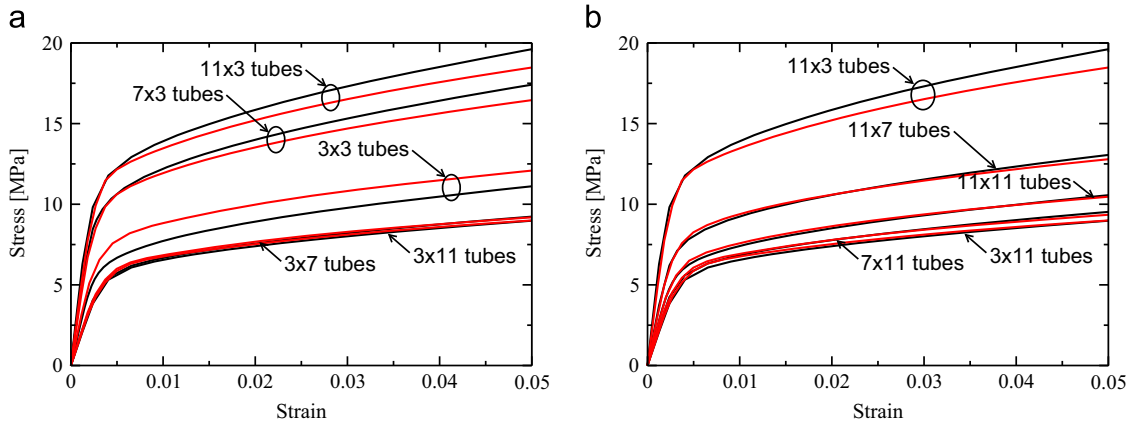

Fig. 17. Stress–strain curves predicted by both the full-scale simulations (black curves) and the HEM-based ones (red curves) for sandwich structures made of a square stacking core (compressive load). Comparison with: (a) the 3×3-tube core, (b) the 11×11-tube core (width $\times$ height). (For interpretation of the references to colour in this figure caption, the reader is referred to the web version of this paper.)

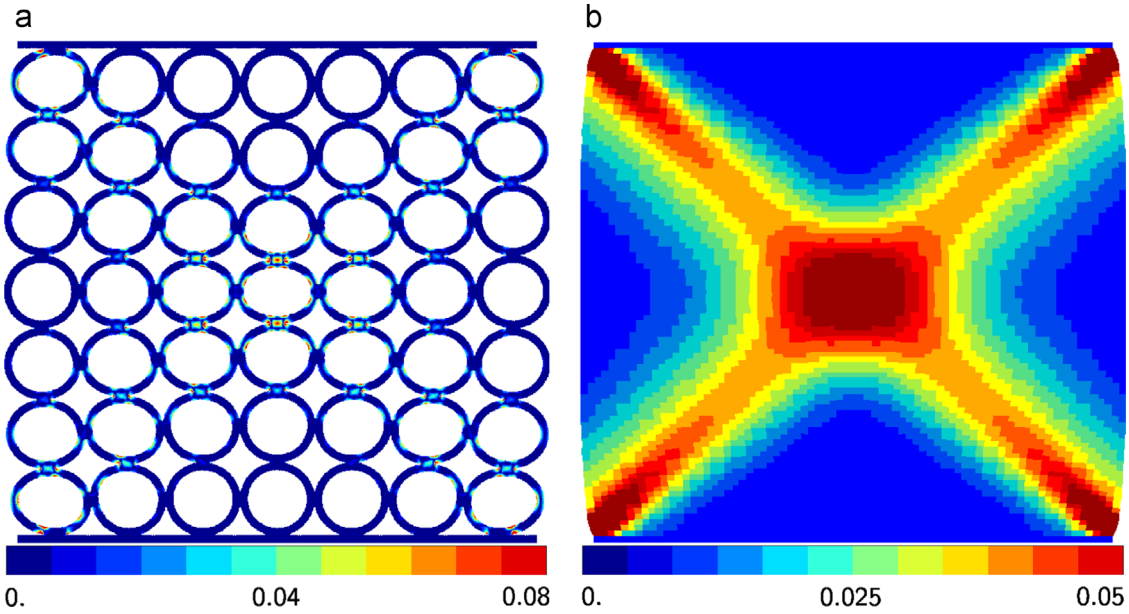

Fig. 18. Deformed maps of cumulated plastic strain of square stacking sandwich structures of a 7×7 tubes; (a) full-scale model, (b) HEM-based model. Note that the two models have a different plastic strain measure as the full scale model has a very localised plastic strain and the HEM is homogeneous. The maps are plotted in terms of integration node values.

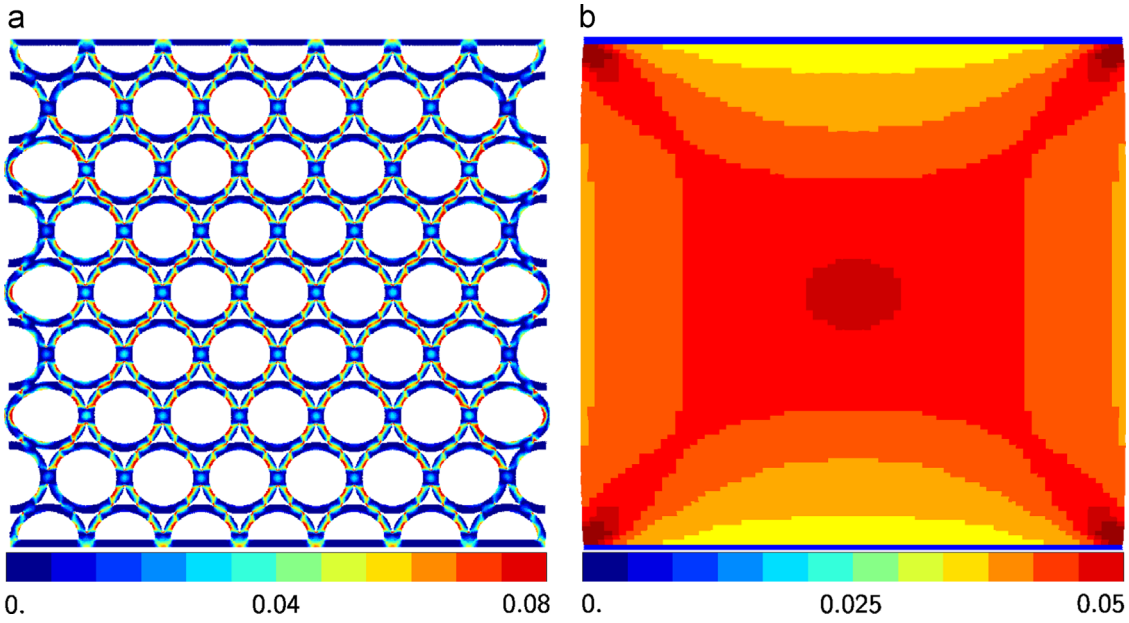

Fig. 19. Deformed maps of cumulated plastic strain of hexagonal stacking sandwich structures of a 7×7 tubes; (a) full-scale model, (b) HEM-based model. Note that the two models have a different plastic strain measure as the full scale model has a very localised plastic strain and the HEM is homogeneous. The maps are plotted in terms of integration node values.

structures under various loading cases. For that purpose, sandwich structures made of a tube stacking core have been considered as model cellular structures. Two different tube stacking cores have been simulated, e.g. square or hexagonal, and two different loading cases have been applied, e.g. uni-axial transverse compression and in-plane simple shear. From a macroscopic point of view those simple loading cases are interesting because of the local multi-axial stress states observed in the cores resulting from both the heterogeneity of the sandwich structure and the boundary layer effects. The following conclusions can be drawn:

- first, the tube stacking cores have been characterised in detail by simulating multi-axial loading cases on the representative volume elements of the stackings through the finite element method. These simulations show significant differences between the two stacking patterns in terms of anisotropy and shape of their yield surfaces. Especially, the braze joints between the tubes and their orientation towards the load direction play a significant role in the anisotropy of the tube stacking behaviour. The simulations also highlight the very strong in-plane/out-of-plane anisotropy of such cellular structures resulting from their extruded character, hence some difficulties to model both in-plane and out-of-plane behaviours by using only one plastic potential. However, in the restricted case of in-plane behaviours, a very good fit has been obtained between the mechanical behaviours simulated on the unit cells of both tube stackings and those predicted by the identified HELs;

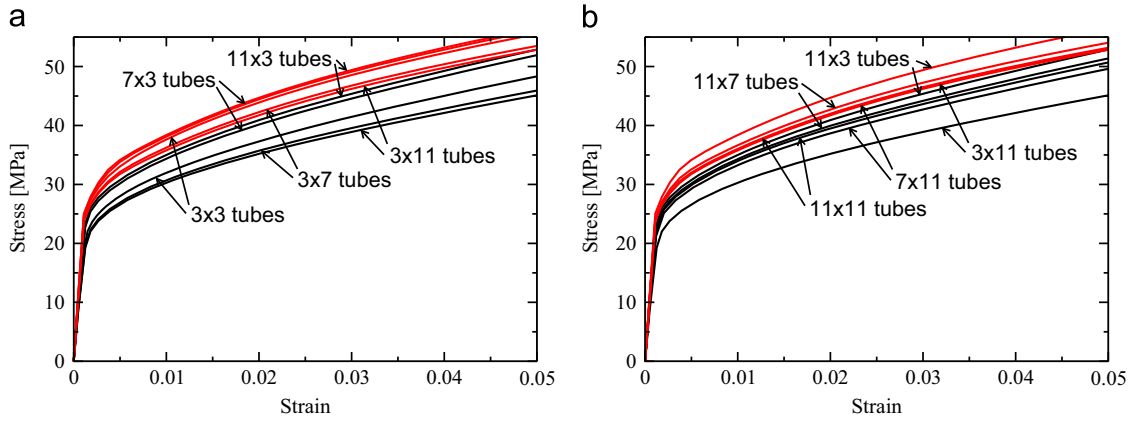

Fig. 20. Stress–strain curves predicted by both the full-scale simulations (black curves) and the HEM-based ones (red curves) for sandwich structures made of a finite periodic hexagonal stacking core (compressive load). Comparison with: (a) the 3×3-tube core, (b) the 11×11-tube core (width $\times$ height). (For interpretation of the references to colour in this figure caption, the reader is referred to the web version of this paper.)

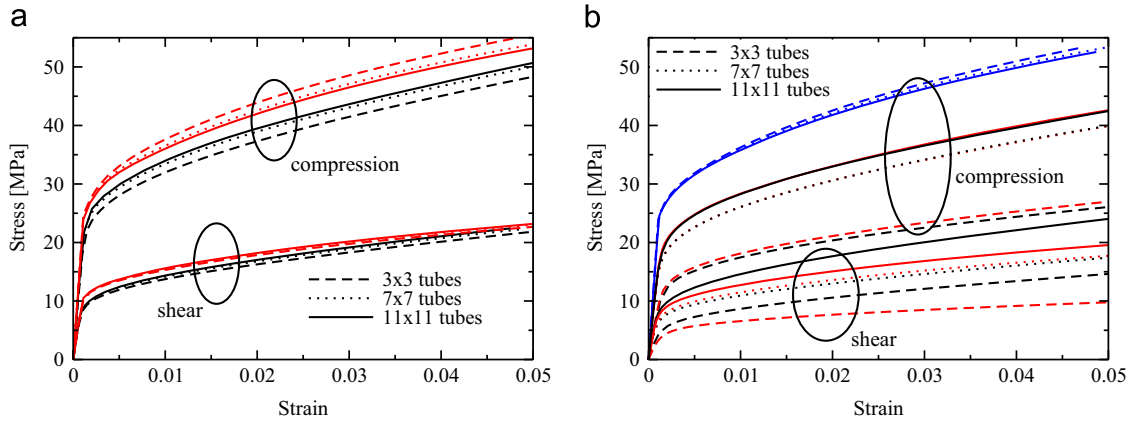

Fig. 21. Comparison between the mechanical responses predicted by both the full-scale modelling (black curves) and the HEM-based one (red curves) in the case of: (a) the fully periodic hexagonal stacking core, (b) the non-fully periodic hexagonal stacking core (blue curves are the ones that were obtained when replacing all the core with its HEM in that case), for both compressive and simple shear loads. (For interpretation of the references to colour in this figure caption, the reader is referred to the web version of this paper.)

- then, the identified HELs have been evaluated by simulating finite sandwich structures consisting of a tube stacking core between two skins in which the core was replaced with its HEM. The results of these simulations have been compared to those obtained on the reference full-scale structures. Even if some limitations are observed in the case of the hexagonal pattern, the simulations performed in various geometrical configurations show the relevance of the HELs identified for the modelling of sandwich structures made of tube stacking cores. The results of the HEM-based simulations are very close to those of the full-scale modelling for most architectures with considerably lower computational costs (for instance, the gain is about a factor of 300 in the case of the 7×7-square stacking core).
- furthermore, the results obtained highlight significant boundary layer effects too. Two different antagonistic effects are observed resulting on one side from the containment effect of the skins and, on the other side, from the lateral free edges of the structure. Thus different trends have been identified in terms of core size effect on the effective strength of the sandwich structures, depending on the stacking pattern and the main boundary layer effect that govern the mechanical response;
- nevertheless, the HEM-based approach detailed here still presents some limitations when the assumption of the scale separation is no longer verified or for instance when locally the RVE of the cellular core is no more respected for technological or processing reasons. Even if these effects are expected to vanish when increasing the core size, one possible way to prevent them could be the use of generalised continuum media such as done for instance in [56–59].

Here, the macroscopic strain levels have been limited to 5% for reasons of validity of the HELs identified in small deformations. Obviously, locally the microscopic cumulated plastic strain levels can be considerably higher in the tube stackings. Even if this preliminary study provides interesting results concerning the effective plastic behaviour of such cellular structures, some works are in progress to extend this approach to large deformations and to address the modes of instability that can occur at larger strain levels. Moreover, even if the HEM-based approach developed here on tube stackings can be extended to many other cellular architectures, it is worth noting that a universal yield criterion does probably not exist for all cellular architectures. The yield criterion must be adapted to the specific features of each cellular architecture.

Acknowledgements

We are indebted to our colleagues B. Langrand and G. Portemont for many fruitful discussions. This work has been supported thanks to the framework of the Carnot institutes.

References

[1] Evans AG, Hutchinson JW, Ashby MF. Multifunctionality of cellular metal systems. Progr Mater Sci 1998;43(3):171–221.
[2] Silva MJ, Hayes WC, Gibson LJ. The effects of non-periodic microstructure on the elastic properties of two-dimensional cellular solids. Int J Mech Sci 1995;37(11):1161–77.
[3] Silva MJ, Gibson LJ. The effects of non-periodic microstructure and defects on the compressive strength of two-dimensional cellular solids. Int J Mech Sci 1997;39(5):549–63.
[4] Fazekas A, Dendievel R, Salvo L, Bréchet Y. Effect of microstructural topology upon the stiffness and strength of 2D cellular structures. Int J Mech Sci 2002;44(10):2047–66.
[5] Sanders WS, Gibson LJ. Mechanics of hollow sphere foams. Mater Sci Eng A 2003;347:70–85.
[6] Sanders WS, Gibson LJ. Mechanics of BCC and FCC hollow-sphere foams. Mater Sci Eng A 2003;352:150–61.
[7] Marcadon V, Kruch S. Influence of geometrical defects on the mechanical behaviour of hollow-sphere structures. Int J Solids Struct 2013;50:498–510.
[8] Amsterdam E, de Vries JHB, de Hosson JThM, Onck PR. The influence of strain-induced damage on the mechanical response of open-cell aluminum foam. Acta Mater 2008;56:609–18.
[9] Amsterdam E, de Hosson JThM, Onck PR. On the plastic collapse stress of open-cell aluminum foam. Scr Mater 2008;59:653–6.
[10] Mangipudi KR, Onck PR. Multiscale modelling of damage and failure in two-dimensional metallic foams. J Mech Phys Solids 2011;59:1437–61.
[11] Marcadon V, Feyel F. Modelling of the compression behaviour of metallic hollow-sphere structures: about the influence of their architecture and their constitutive material's equations. Comput Mater Sci 2009;47(2):599–610.
[12] Marcadon V, Kruch S. Roles of mechanical heterogeneities and damage on the overall mechanical behaviour of hollow-tube stackings. Proc Eng 2011;10:2815–20.
[13] Dillard T, Forest S, Ienny P. Micromorphic continuum modelling of the deformation and fracture behaviour of nickel foams. Eur J Mech A/Solids 2006;25(3):526–49.
[14] Fallet A, Lhuissier P, Salvo L, Bréchet Y. Mechanical behaviour of metallic hollow spheres foam. Adv Eng Mater 2008;10:858–62.
[15] Lhuissier P, Fallet A, Salvo L, Bréchet Y. Quasistatic mechanical behaviour of stainless steel hollow sphere foam: macroscopic properties and damage mechanisms followed by X-ray tomography. Mater Lett 2009;63(13):1113–6.
[16] Burteau A, N'Guyen F, Bartout JD, Forest S, Bienvenu Y, Saberi S, et al. Impact of material processing and deformation on cell morphology and mechanical behavior of polyurethane and nickel foams. Int J Solids Struct 2012;49:2714–32.
[17] Gasser S, Paun F, Riffard L, Bréchet Y. Microplastic yield condition for a periodic stacking of hollow spheres. Scr Mater 2004;50(4):401–5.
[18] Alkhader M, Vural M. An energy-based anisotropic yield criterion for cellular solids and validation by biaxial FE simulations. J Mech Phys Solids 2009;57(5):871–90.
[19] Hönig A, Stronge WJ. In-plane dynamic crushing of honeycomb. Part I: crush band initiation and wave trapping. Int J Mech Sci 2002;44(8):1665–96.
[20] Blazy JS, Marie-Louise A, Forest S, Chastel Y, Pineau A, Awade A, et al. Deformation and fracture of aluminium foams under proportional and non proportional multi-axial loading: statistical analysis and size effect. Int J Mech Sci 2004;46(2):217–44.
[21] Marcadon V, Davoine C, Passilly B, Boivin D, Popoff F, Rafray A, et al. Mechanical behaviour of hollow-tube stackings: experimental characterization and modelling of the role of their constitutive material behaviour. Acta Mater 2012;60(15):5626–44.
[22] Hayes AM, Wang A, Dempsey BM, McDowell DL. Mechanics of linear cellular alloys. Mech Mater 2004;36(8):691–713.
[23] Papka SD, Kyriakides S. Biaxial crushing of honeycombs: Part I: experiment. Int J Solids Struct 1999;36(29):4367–96.
[24] Papka SD, Kyriakides S. Biaxial crushing of honeycombs: Part II: analysis. Int J Solids Struct 1999;36(29):4397–423.
[25] Caty O, Maire E, Youssef S, Bouchet R. Modeling the properties of closed-cell cellular materials from tomography images using finite shell elements. Acta Mater 2008;56(19):5524–34.
[26] Ostoja-Starzewski M. Material spatial randomness: from statistical to representative volume element. Probab Eng Mech 2006;21(2):112–32.
[27] Wang AJ, McDowell DL. Yield surfaces of various periodic metal honeycombs at intermediate relative density. Int J Plast 2005;21(2):285–320.
[28] Ajdari A, Canavan P, Nayeb-Hashemi H, Warner G. Mater Sci Eng A 2009;499:434–9.
[29] Simone AE, Gibson LJ. Effects of solid distribution on the stiffness and strength of metallic foams. Acta Mater 1998;46(6):2139–50.
[30] Florence C, Sab K. A rigorous homogenization method for the determination of the overall ultimate strength of periodic discrete media and an application to general hexagonal lattices of beams. Eur J Mech A/Solids 2006;25(1):72–97.
[31] Harders H, Hupfer K, Rösler J. Influence of cell wall shape and density on the mechanical behaviour of 2D foam structure. Acta Mater 2005;53(5):1335–45.
[32] Xue Z, Hutchinson JW. Constitutive model for quasi-static deformation of metallic sandwich cores. Int J Numer Methods Eng 2004;61(13):2205–38.
[33] Styles M, Compston P, Kalyanasundaram S. Finite element modelling of core thickness effects in aluminium foam/composite sandwich structures under flexural loading. Compos Struct 2008;86(1):227–32.
[34] Feyel F, Chaboche JL. FE2 multiscale approach for modelling the elastovisco-plastic behaviour of long fibre SiC/Ti composite materials. Comput Methods Appl Mech Eng 2000;183(3):309–30.
[35] Kouznetsova V, Brekelmans WAM, Baaijens FPT. An approach to micro-macro modeling of heterogeneous materials. Comput Mech 2001;27(1):37–48.
[36] Kouznetsova V, Geers MGD, Brekelmans WAM. Multi-scale constitutive modelling of heterogeneous materials with a gradient-enhanced computational homogenization scheme. Int J Numer Methods Eng 2002;54(8):1235–60.
[37] Combaz E, Bacciarini C, Charvet R, Dufour W, Dauphin F, Mortensen A. Yield surface of polyurethane and aluminium replicated foam. Acta Mater 2010;58(15):5168–83.
[38] Wang DA, Pan J. A non-quadratic yield function for polymeric foams. Int J Plast 2006;22(3):434–58.
[39] Deshpande VS, Fleck NA. Isotropic constitutive models for metallic foams. J Mech Phys Solids 2000;48(6):1253–83.
[40] Tsuda M, Takemura E, Asada T, Ohno N, Igari T. Homogenized elastic-viscoplastic behavior of plate-fin structures at high temperatures: numerical analysis and macroscopic constitutive modeling. Int J Mech Sci 2010;52(5):648–56.
[41] Hill R. A theory of the yielding and plastic flow of anisotropic metals. Proc R Soc Lond Ser A Math Phys Sci 1948;193(1033):281–97.
[42] Karafillis AP, Boyce M. A general anisotropic yield criterion using bounds and a transformation weighting tensor. J Mech Phys Solids 1993;41(12):1859–86.
[43] Barlat F, Lege DJ, Brem JC. A six-component yield function for anisotropic materials. Int J Plast 1991;7(7):693–712.
[44] Bron F, Besson J. A yield function for anisotropic materials application to aluminum alloys. Int J Plast 2004;20(4):937–63.
[45] Green RJ. A plasticity theory for porous solids. Int J Mech Sci 1972;14(4):215–24.
[46] Badiche X, Forest S, Guibert T, Bienvenu Y, Bartout JD, Ienny P, et al. Mechanical properties and non-homogeneous deformation of open-cell nickel foams: application of the mechanics of cellular solids and of porous materials. Mater Sci Eng A 2000;289:276–88.
[47] Hill R. The essential structure of constitutive laws for metal composites and polycrystals. J Mech Phys Solids 1967;15(2):75–95.
[48] Suquet P. Elements of homogenization for inelastic solid mechanics. Homog Tech Compos Media 1987;272:193–278.
[49] Michel JC, Moulinec H, Suquet P. Effective properties of composite materials with periodic microstructure: a computational approach. Comput Methods Appl Mech Eng 1999;172:109–43.
[50] Ohno N, Ikenoya K, Okumura D, Matsuda T. Homogenized elastic-viscoplastic behavior of anisotropic open-porous bodies with pore pressure. Int J Solids Struct 2012;49:2799–806.
[51] Besson J, Cailletaud G, Chaboche JL, Forest S, Blétry M. Non-linear mechanics of materials, series: solid mechanics and its applications, vol. 167. Heidelberg: Springer; 2009.
[52] Von Mises R. Mechanik der plastischen Formänderung von Kristallen. ZAMM—J Appl Math Mech 1928;8:161–85.
[53] Cailletaud G, Sai K. Study of plastic/viscoplastic models with various inelastic mechanisms. Int J Plast 1995;11(8):991–1005.
[54] Kruch S, Forest S. Computation of coarse grain structures using a homogeneous equivalent medium. J Phys IV 1998;8 Pr8-197-205.
[55] Panasenko GP. Partial homogenization. C R Méc 2002;330(10):667–72.
[56] Forest S. Mechanics of generalized continua: construction by homogenizaton. J Phys IV 1998;8(Pr4) Pr4-39.
[57] Forest S, Sab K. Cosserat overall modeling of heterogeneous materials. Mech Res Commun 1998;25(4):449–54.
[58] Forest S, Sievert R. Elastoviscoplastic constitutive frameworks for generalized continua. Acta Mech 2003;160(1–2):71–111.
[59] Forest S, Trinh DK. Generalized continua and non-homogeneous boundary conditions in homogenisation methods. ZAMM—J Appl Math Mech/Z Angew Math Mech 2011;91(2):90–109.